Neuron, Vol. 43, 779–793, September 16, 2004, Copyright ©2004 by Cell Press

# The Transcription Factor *Bhlhb4* Is Required for Rod Bipolar Cell Maturation

**Debra E. Bramblett,[1,*] Mark E. Pennesi,[2,3] Samuel M. Wu,[2,3] and Ming-Jer Tsai[1,4]**
[1]Department of Molecular and Cellular Biology
[2]Department of Ophthalmology
[3]Division of Neuroscience
[4]Program in Developmental Biology
Baylor College of Medicine
Houston, Texas 77030

## Summary

**Retinal bipolar cells are essential to the transmission of light information. Although bipolar cell dysfunction can result in blindness, little is known about the factors required for bipolar cell development and functional maturation. The basic helix-loop-helix (bHLH) transcription factor *Bhlhb4* was found to be expressed in rod bipolar cells (RB). Electroretinograms (ERGs) in the adult *Bhlhb4* knockout (*Bhlhb4*$^{-/-}$) showed that the loss of *Bhlhb4* resulted in disrupted rod signaling and profound retinal dysfunction resembling human congenital stationary night blindness (CSNB), characterized by the loss of the scotopic ERG b-wave. A depletion of inner nuclear layer (INL) cells in the adult *Bhlhb4* knockout has been ascribed to the abolishment of the RB cell population during postnatal development. Other retinal cell populations including photoreceptors were unaltered. The timing of RB cell depletion in the *Bhlhb4*$^{-/-}$ mouse suggests that *Bhlhb4* is essential for RB cell maturation.**

## Introduction

The processing of visual information involves a network of primary, secondary, and tertiary neurons and glial cells in the retina prior to its transmission to the brain. The development and maintenance of the neuronal circuitry of the mouse retina has been a hot topic under intensive investigation recently (Peachey and Ball, 2003). A large number of mouse mutant retinal phenotypes resembling human visual impairment conditions exist, and many of these involve degeneration of the first-order neurons of the retina, the photoreceptor cells, while only a few mouse models displaying defects in secondary retinal neuron development have been reported. Until now, no mouse models have been described in which the disruption of a single transcriptional regulator gene, specifically required for the maturation of retinal rod bipolar (RB) cells, results in the profound loss of retinal function and therefore vision.

Rod and cone photoreceptors transmit light information gathered by their outer and inner photoreceptive segments to bipolar cells and horizontal cells, which reside in the second nuclear layer, or the inner nuclear layer (INL) (for review, see Sterling, 1998). Bipolar and horizontal processes extend outward into the outer plexiform layer (OPL) to invaginate into the photoreceptor terminals that form ribbon synapses. Bipolar cells then transmit the signal to retinal ganglion cells (RGCs) and amacrine cells by extending axons into the inner plexiform layer (IPL). RGCs populate the third and innermost nuclear layer, the ganglion cell layer (GCL), and their axons form the optic nerve.

One RB cell type and nine cone bipolar (CB) cell types have been characterized based on their cellular morphology, particularly the stratification layer of the IPL where their axons terminate and whether they depolarize (ON) or hyperpolarize (OFF) in response to changes in glutamate release from the photoreceptors in response to light (Ghosh et al., 2004; Pang et al., 2004). RB cells serve low light (starlight), are all of the ON variety, and relay light information to RGCs only indirectly through AII amacrine cells. RB cells are distinguished by the fact that their axons descend to the deepest stratum of the IPL, where their globular terminals contact the processes of AII amacrine cells via ribbon synapses. The AII amacrine cells then make use of the direct connections made by CB cells to relay the rod signal to the RGCs by forming inhibitory synapses with OFF CB cells and excitatory synapses with ON CB cells (Bloomfield and Dacheux, 2001; Strettoi et al., 1990, 1992). Thus, RB cells are essential elements for the visual process, and without them there is partial blindness.

Mouse retinal development begins midway through embryogenesis (E10), but it proceeds well into the postnatal (P) period until eye opening around P14 (Cepko et al., 1996). The bulk of the bipolar cell population arises during the latter half of retinal development. Retinal progenitor cells have the capacity to differentiate into each of the major retinal neurons and glia. Establishment of the appropriate composition of retinal cell types is likely achieved by progressive changes in the tendencies for the retinal progenitors to proceed down one retinal cell pathway versus another over time. This change in propensity is based, in part, on the complement of transcriptional regulators that are expressed in that particular window of time. Thus, the development of the retina is dependent upon an appropriate time course of gene regulation during development, in which basic helix-loop-helix (bHLH) transcriptional regulators and homeodomain transcription factors play major roles (Pennesi et al., 2003; Hatakeyama et al., 2001; De Melo et al., 2003; Akagi et al., 2004).

Bipolar cell fate specification is dependent upon the combined action(s) of the homeodomain factor *Chx10* and the bHLH factors *Mash1* and *Math3* (Burmeister et al., 1996; Hatakeyama et al., 2001). *Chx10* is expressed in bipolar progenitor cells and later its expression becomes segregated to a bipolar cell subpopulation (Liu et al., 1994). The loss of the *Chx10* gene results in the complete loss of bipolar cells in mice, suggesting that *Chx10* is required for bipolar cell development (Burmeister et al., 1996). However, when *Chx10* is overexpressed, the INL cell number increases, but those cells induced by *Chx10* are Müller glia and undifferentiated bipolar cells and none are mature bipolar cells (Hatakeyama et

*Correspondence: debrab@bcm.tmc.edu

al., 2001). Thus, *Chx10* alone is not sufficient for bipolar cell differentiation. Rather, *Chx10* must be overexpressed together with either of the bHLH factors *Mash1* or *Math3* to significantly promote bipolar cell specification (Hatakeyama et al., 2001). Overexpression of *Chx10* together with the bHLH repressor *Hes5* results in an induction of Müller glial cells, increased over the induction observed with *Chx10* overexpression alone. Thus, it appears that *Chx10* does not determine the retinal neuron cell fate, rather it dictates INL specificity (Hatakeyama et al., 2001). By the same token, overexpression of either *Mash1* or *Math3* alone results in the induction of rod photoreceptors but not bipolar cells, indicating that these bHLH factors can induce neuronal differentiation but that each gene alone is insufficient for bipolar specification (Hatakeyama et al., 2001). Furthermore, not all cells overexpressing *Chx10* together with *Mash1* or *Math3* become bipolar cells, suggesting that other factors are necessary for subtype specification (Hatakeyama et al., 2001).

Bipolar cell subtype specification and functional maturation and maintenance likely require a combinatorial code of homeodomain and bHLH transcriptional regulators. We have recently described a bHLH factor, *Bhlhb4*, which is expressed in a highly regionalized fashion in the nervous system and retina during development and in the adult (Bramblett et al., 2002, and herein). Evidence of high *Bhlhb4* expression in the retina and the neuronal cell type-specific transcriptional activation by *Bhlhb4* in transient transfections (data not shown) lead us to predict that *Bhlhb4* may also play a role in neural development of the retina. Loss of *Bhlhb4* resulted in a profound deficit in retinal activity that was attributed to the abolishment of the RB cell population. Our data are consistent with *Bhlhb4* regulating aspects of neuronal maturation of RB cells during retinal development, and failure to achieve these aspects of RB cell maturation lead to cell death in the *Bhlhb4* knockout.

## Results

### Generation of the *Bhlhb4* Knockout

The *Bhlhb4*$^{-/-}$ animal was generated in order to determine the in vivo function of *Bhlhb4* (Figures 1A and 1B, see Experimental Procedures). Heterozygous matings yielded the *Bhlhb4*$^{-/-}$, *Bhlhb4*$^{+/-}$, and wild-type (wt) mice at a frequency corresponding to a normal Mendelian ratio, indicating that the loss of *Bhlhb4* did not result in an embryonic lethal phenotype. In situ hybridization performed on sections of E12.5 wt and *Bhlhb4*$^{-/-}$ embryos demonstrated the complete absence of the *Bhlhb4* mRNA in the *Bhlhb4*$^{-/-}$ brain and retina (Figures 1E–1H and data not shown). Signal corresponding to *Bhlhb4* transcripts was observed in the E12.5 wt pretectal region (Figure 1E), while no signal was detected in the *Bhlhb4* knockout (Figure 1G).

The *Bhlhb4*$^{-/-}$ animals survived through adulthood, allowing for the examination of adult physiology and function in addition to that of the developing animal. The adult *Bhlhb4*$^{-/-}$ brain was indistinguishable from the wt in size and gross morphology (data not shown). Examination of a variety of neuronal markers by in situ hybridization on developing embryonic brain and neural tube (*Pax6, Lim-1, Gbx2, Ngn2, TCF4, Wnt3, Nkx2.2, Nkx6.1, Tal2*) demonstrated that the regionalization of the *Bhlhb4*$^{-/-}$ diencephalon, where *Bhlhb4* is highly expressed, was not significantly changed in the *Bhlhb4*$^{-/-}$ mouse (unpublished data).

### Examination of *Bhlhb4* Expression

Replacement of the *Bhlhb4* coding region with the *LacZ* reporter gene allowed the *Bhlhb4* expression pattern to be tracked easily. Strong, highly cell type-specific *Bhlhb4-LacZ* expression was detected in the adult retina (Figure 1R) and in the pretectal region of the embryonic (data not shown) and adult brain (Figure 1S). The *Bhlhb4-lacZ* expression mimicked that of the endogenous *Bhlhb4* mRNA in the brain and the retina (Figure 1Q versus 1R and data not shown), indicating that the *Bhlhb4-LacZ* knockin was representative of normal *Bhlhb4* expression. In the adult retina, both the *Bhlhb4* mRNA and *Bhlhb4-LacZ* expression were detected prominently at the top/outer edge of the INL, a position that resembled that of RB cells, and neither LacZ staining nor *Bhlhb4* mRNA signal was observed in the GCL or in the outer nuclear layer (ONL) (Figure 1R).

In the postnatal retina (Figure 1I–1P), *Bhlhb4* mRNA expression was detected in a restricted population of cells in the INL as early as P5 by in situ hybridization (Figure 1I). The *Bhlhb4* mRNA signal gradually increased between P5 and P8, peaking at P8 (Figure 1L), shifting from the lower edge to the outer edge of the INL and becoming more compact (Figures 1I–1K). The signal dramatically dropped off at P9 such that by P10 it was nearly undetectable, and it was gone by P12 (Figures 1M–1O). *Bhlhb4-LacZ* was expressed in a similar fashion, as detected by immunofluorescent (IF) labeling (see below), except that β-galactosidase protein (β-gal) could be detected at P10, likely due to high β-gal protein stability (24–48 hr), but was difficult to detect at P12 or before P7 (Figure 8 and data not shown). *Bhlhb4* transcripts were detected again at P14, around the time the eyes open (Figure 1P), but at more moderate levels, which were maintained in the adult (Figure 1Q). Thus, *Bhlhb4* likely has both a developmental role and a role in the adult retina.

### Electroretinograms Revealed Profound Retinal Dysfunction in *Bhlhb4*$^{-/-}$ Mice

To assess retinal function, a series of noninvasive scotopic and photopic electroretinogram (ERG) experiments were conducted on *Bhlhb4*$^{+/-}$, *Bhlhb4*$^{-/-}$, and wt (+/+) littermates between 1 and 2 months of age (Figure 2). Under scotopic conditions (dim light), the ERG detects responses from rod-driven circuitry, while under photopic (day light) conditions, it detects responses from cone-driven circuitry. The scotopic b-wave is the extracellular field potential that primarily arises from RB cells in response to dim flashes of light (Pugh et al., 1998). Figures 2A–2C show scotopic b-wave responses to increasing intensities of flashed light. The relationship between scotopic b-wave amplitude and intensity can be modeled using a hyperbolic saturation function (Naka-Rushton). This model yields two parameters, $b_{max,\,scot}$ and $I_{0.5}$, representing the maximum b-wave amplitude and the intensity that provides half saturation (Ta-

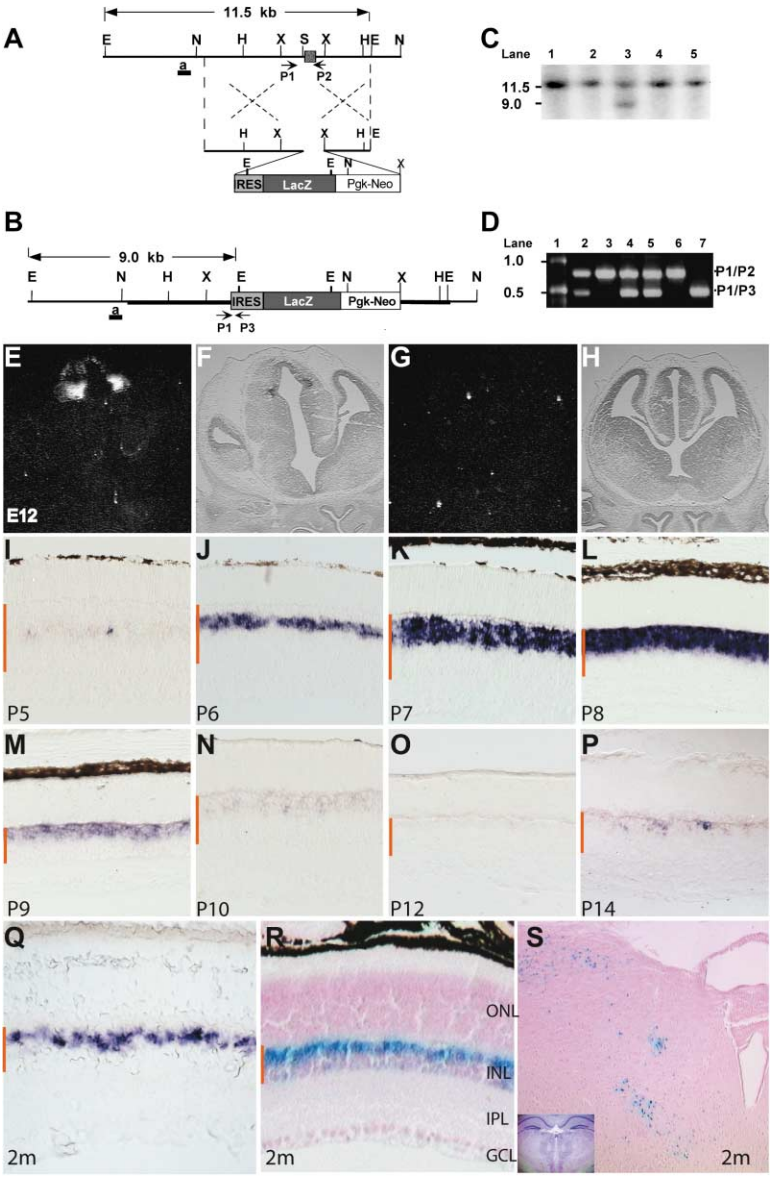


Figure 1. Generation of the *Bhlhb4* Knockout Mouse and Determination of the *Bhlhb4* Expression Pattern

(A) *Bhlhb4* locus restriction map (top) and targeting construct (below) with homologous regions flanking a reporter/selection gene cassette (IRES-LacZ/PgkNeo-loxp). The stippled gray box is the *Bhlhb4* coding region. (B) Map of correctly targeted allele. (C) Representative Southern blot of ES cell clone DNA screened for targeted *Bhlhb4* alleles. Probe "a" detected the 9 kb EcoRI fragment (KO) or an 11.5 kb EcoRI fragment (wt). (D) Representative PCR genotype screen of a litter from a heterozygous mating: *Bhlhb4*$^{+/-}$ (lanes 2, 4, and 5), wild-type (lanes 3 and 6), knockout (lane 7). P1 and P2 PCR primers amplified the wild-type allele. P1 and P3 PCR primers amplified the targeted allele. The sizes (in kb) of the DNA fragments are indicated. (E–H) Radioactive in situ hybridization using a *Bhlhb4* riboprobe on wt (E and F) and *Bhlhb4*$^{-/-}$ (G and H) E12.5 embryos. Corresponding brightfield images (F and H) to the darkfield views (E and G) are shown. (I–Q) Colorimetric in situ hybridization (purple) on retinal sections (from central retina). Red bars indicate the INL, and the postnatal ages are indicated. (R) LacZ staining (blue) of the adult retina and the pretectal region of the adult brain (S) with nuclear fast red counterstain. Inset in (S) shows cresyl violet-stained adjacent section of the adult brain for positional reference.

ble 1). In wild-type mice, $b_{max,\ scot}$ measured about 640 $\mu$V and $I_{0.5}$ = 2.0 $\phi$/rod. *Bhlhb4*$^{+/-}$ mice demonstrated a small but significant ($p < 0.01$, Student's t test, two-tailed) decrease in the scotopic b-waves, with $b_{max,\ scot}$ averaging 485 $\mu$V. Scotopic b-wave recordings from *Bhlhb4*$^{-/-}$ mice were profoundly decreased, with $b_{max,scot}$ measuring only 165 $\mu$V. Responses were absent at the lowest intensities and were greatly diminished at higher intensities.

We measured the ERG a-wave, which in the mouse under scotopic conditions arises almost exclusively from the rod photoreceptors (Pugh et al., 1998). Figures 2D–2F show the response to an intense flash that saturated the rod photoreceptors. Wild-type mice produced a saturated a-wave, or $a_{max,\ scot}$, measuring about 825 $\mu$V (Table 1). In *Bhlhb4*$^{+/-}$ and *Bhlhb4*$^{-/-}$ mice, the saturated a-wave measured 700 $\mu$V and 825 $\mu$V, respectively. There was no significant difference between wild-type, *Bhlhb4*$^{+/-}$, or *Bhlhb4*$^{-/-}$ mice. To analyze the amplification of the rod transduction cascade, a series of a-waves to different intensities were fit (Hood and Birch, 1994) (Figures 2G–2I and Table 1). There was no significant difference between wt, *Bhlhb4*$^{+/-}$, or *Bhlhb4*$^{-/-}$ mice.

The integrity of the rod photoreceptor population was confirmed by IF labeling of retinas from 3-, 5-, and 6-month-old wt and *Bhlhb4*$^{-/-}$ animals with anti-rhodopsin antibodies. The rhodopsin expression and the number of photoreceptor cells in the ONL were similar in both genotypes and remained constant up to 6 months of age (data not shown). These results together with the ERG data suggested that photoreceptor outer segment function remained intact and that the observed disruption in the rod photo transmission circuitry was at the level of the RB cells.

To determine cone-driven function, we measured the ERG response to an intense flash of light in the presence of a rod-suppressing background light (Figures 2J–2L and Table 1). Recordings from wt and *Bhlhb4*$^{+/-}$ mice

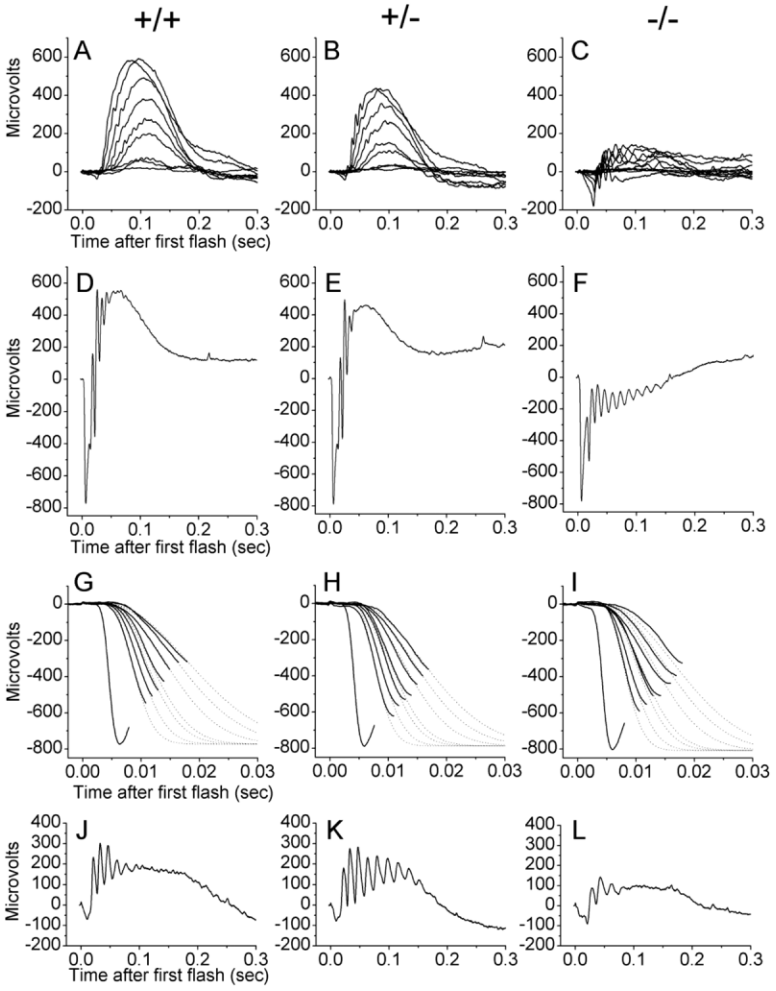


Figure 2. Examination of Retinal Activity by Electroretinogram

Representative ERGs from wild-type (+/+), heterozygous (+/−), and *Bhlhb4*$^{-/-}$ (−/−) mice are shown. (A–C) Scotopic b-wave. Traces were obtained using a series of 500 nm flashes with intensities ranging from −3.86 to −1.76 log scot cd s m$^{-2}$ (estimated to produce between 0.13 to 16.1 photoisomerizations/rod in photoreceptors with normal outer segments). Each trace represents the average of at least five flashes. (D–F) ERG response to an intense flash (2.92 log scot cd s m$^{-2}$ or an estimated 800,000 photoisomerizations/rod) used to measure the saturated a-wave amplitude. (G–I) The a-wave response to flashes varying in intensity from −0.51 log scot cd s m$^{-2}$ 2.92 log scot cd s m$^{-2}$ (290 to 800,000 photoisomerizations/rod). Traces have been fit using the Lamb-Pugh model. There was no significant difference in the amplification coefficient between control, *Bhlhb4*$^{+/-}$, or *Bhlhb4*$^{-/-}$ mice. (J–L) Cone-driven ERGs in response to an intense white flash (estimated to produce 800,000 photoisomerizations/rod in darkness) in the presence of a rod suppressing 540 nm background (estimated to produce 40 phot cd m$^{-2}$). Each trace represents the average of ten trials. There was no significant difference in b-wave amplitude between (+/+) and (+/−) mice. Cone-driven b-wave amplitudes were slightly reduced in (−/−) mice.

were indistinguishable. There was a slight reduction in the maximum amplitude of photopic b-wave in the *Bhlhb4*$^{-/-}$ mice as compared to wt. Thus, the loss of *Bhlhb4* had an effect on CB activity, although incomplete. Interestingly, the a-waves were more visible in the *Bhlhb4*$^{-/-}$ mice at higher intensities, possibly reflecting an unmasking effect due to the loss of the rod-driven b-wave (Table 1).

### The Basis of the Disruption of the Rod Circuitry in *Bhlhb4*$^{-/-}$ Retina

The dramatic loss of RB cell activity in the *Bhlhb4*$^{-/-}$ mice by itself suggested several possibilities. The loss of *Bhlhb4* could have resulted in a nonfunctional population of RB cells that were unable to receive the transmission of signals from rod photoreceptors due to alterations at the dendrites. The photoreceptor terminals could have been defective or there could have been a reduction in bipolar cell numbers due to retinal precursor cell failure to generate a particular cell type, to proliferate, or to differentiate properly, leading to programmed cell death (apoptosis).

Although the overall layering of the adult (2- to 3-month-old) *Bhlhb4*$^{-/-}$ retinas was normal, the INL was thinner in the *Bhlhb4*$^{-/-}$ retina in comparison to the wt littermate (Figures 3A and 3B). The positioning and thickness of the remaining two nuclear layers (ONL and GCL) and the inner and outer plexiform layers (IPL and OPL) were similar to the wt. Counting the number of cells in both the INL and the ONL in a defined cross-sectional area from the back/central region of the retina, in similar positions relative to the optic nerve, revealed that the INL cell number in the *Bhlhb4*$^{-/-}$ mice was 21% less than wt (data not shown). INL cell counts were normalized to ONL cell counts for each section to compensate for variations in the angle of sectioning. The reduced INL

Table 1. Summary of ERG Results

| Genotype | $b_{max,\,scot}$ ($\mu$V) | $I_{0.5}$ ($\phi$/rod) | $a_{max,\,scot}$ ($\mu$V) | A (s$^{-2}$) | $b_{max,\,phot}$ ($\mu$V) | $a_{max,phot}$ ($\mu$V) |
|---|---|---|---|---|---|---|
| +/+ (n = 6) | 640 ± 30 | 2.0 ± 0.2 | 825 ± 45 | 3.8 ± 0.3 | 265 ± 35 (n = 4) | 30 ± 3 |
| +/− (n = 6) | 485 ± 40 | 2.9 ± 0.2 | 700 ± 40 | 3.9 ± 0.4 | 230 ± 40 (n = 4) | 30 ± 2 |
| −/− (n = 6) | 165 ± 10 | 3.0 ± 0.5 | 825 ± 30 | 4.3 ± 0.2 | 150 ± 5 (n = 5) | 60 ± 2 |

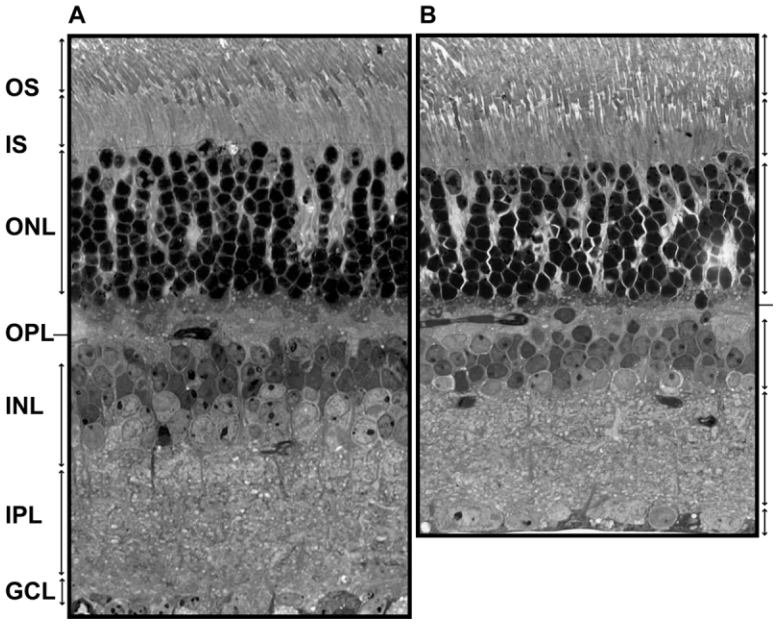


Figure 3. Adult WT and *Bhlhb4*$^{-/-}$ Retina Cross-Sections

(A and B) Plastic thick sections (500 μm) of retinas harvested from wt (A) and *Bhlhb4*$^{-/-}$ (B) 2- to 3-month-old mice. The inner nuclear layer is thinner in the *Bhlhb4*$^{-/-}$ retina (B) than in the wt littermate retina (A). A representative member of each major cell type could be detected in retinas of both genotypes. OS, outer segments; IS, inner segments; ONL, outer nuclear layer; OPL, outer plexiform layer; INL, inner nuclear layer; IPL, inner plexiform layer; GCL, ganglion cell layer.

cell number observed at 2–3 months of age did not appear to be progressive or lead to further degeneration, as the degree of cell loss in the INL was similar in 6-month-old mice (data not shown).

### The *Bhlhb4* Knockout Lacks PKCα-Expressing RB Cells

The visible reduction in cell number in the *Bhlhb4*$^{-/-}$ mice in the INL together with the restricted expression of *Bhlhb4-LacZ* to a subset of cells in the INL suggested that the loss of *Bhlhb4* may have resulted in the loss of one or more INL cell types. There are five major cell types in the mouse retinal INL and at least 42 immunohistologically distinct cell subtypes: one horizontal cell type, 29 different amacrine cell types, Müller cells, RB cells, and nine or ten different CB cell types (Haverkamp and Wassle, 2000). Immunolabeling experiments were performed to visualize each of the major neuronal cell types in the INL of the adult *Bhlhb4*$^{-/-}$ retina and wt littermates (Figures 4–6 and the Supplemental Data [http://www.neuron.org/cgi/content/full/43/6/779/DC1]).

RB cells are specifically labeled by antibodies against protein kinase C-α (PKCα) (Haverkamp and Wassle, 2000). The PKCα$^{+}$ RB somata were located high in the INL, extending a short candelabra-like dendritic arbor into the ONL to collect synaptic input from the rod photoreceptors. The INL is stratified in five layers, S1–S5, and the RB cells extend axons to the innermost layer (S5) of the IPL, ending in large globular terminals, a prominent characteristic of this cell type. Strikingly, RB cells could be visualized in both wt (data not shown) and *Bhlhb4*$^{+/-}$ (Figure 4A) adult retinas, but very few or no cells with RB morphology and expressing PKCα could be detected in cryosections of adult *Bhlhb4*$^{-/-}$ retinas (Figure 4B). Similar results were obtained from labeling whole *Bhlhb4*$^{+/-}$ (Figures 4C–4E) and *Bhlhb4*$^{-/-}$ (Figures 4G–4I) retinas with anti-PKC and observing them in flat mount at several different optical plains. Large numbers of anti-PKCα-labeled somata were present in the control, but only a few oddly shaped cells were present in the *Bhlhb4* knockout. Characteristic globular PKCα$^{+}$ terminals were extremely rare in the *Bhlhb4* knockout (Figure 4I), while in the control they were abundant (Figure 4E). Good estimates of PKCα$^{+}$ cell number can be determined by counting labeled dissociated cells grown in culture. We have chosen to count PKCα$^{+}$ cells in the context of the intact retina, taking advantage of the cellular morphology for RB cell identification on confocal optical sections. Using this method, we estimate that RB cell number was reduced by at least 92% ($p < 0.001$, Student's t test, two-tailed) in the *Bhlhb4*$^{-/-}$ retina as compared to *Bhlhb4*$^{+/-}$ controls (Figure 4F).

A small number of PKCα$^{+}$ cells remained in the *Bhlhb4*$^{-/-}$ INL (Figures 4B, 4G, and 4H). A few of these cells were located at the top of the INL, similar to RB cells, but their axons could not be traced to the IPL. Others rested on the inner edge of the IPL and did not display RB cell morphology (Figures 4B and 4J). Rather, these cells resembled amacrine cells that normally rest on the inner INL edge, have a large soma, and have lateral projections. Surprisingly, the pan-amacrine cell marker *Pax6* is coexpressed with PKCα in the amacrine-like cells in both control (data not shown) and *Bhlhb4*$^{-/-}$ retinas (Figure 4J), suggesting that they are amacrine cells and that PKCα expression may not be restricted solely to the RB population.

The dramatic effect that the loss of *Bhlhb4* had on the RB cell population was highly cell specific. The overall morphology and cell number of several other INL neuronal cell types, including OFF CB cells, horizontal cells, cholinergic starburst amacrine cells, and displaced amacrine cells, labeled by caldendrin, calbindin D, and calretinin (Haverkamp et al., 2003), respectively, were all found to be unchanged in the *Bhlhb4* knockout (see the Supplemental Data [http://www.neuron.org/cgi/content/full/43/6/779/DC1]). Also, stratification of the IPL was observed by IF labeling with anti-calretinin antibodies, which correctly labeled the three striations in

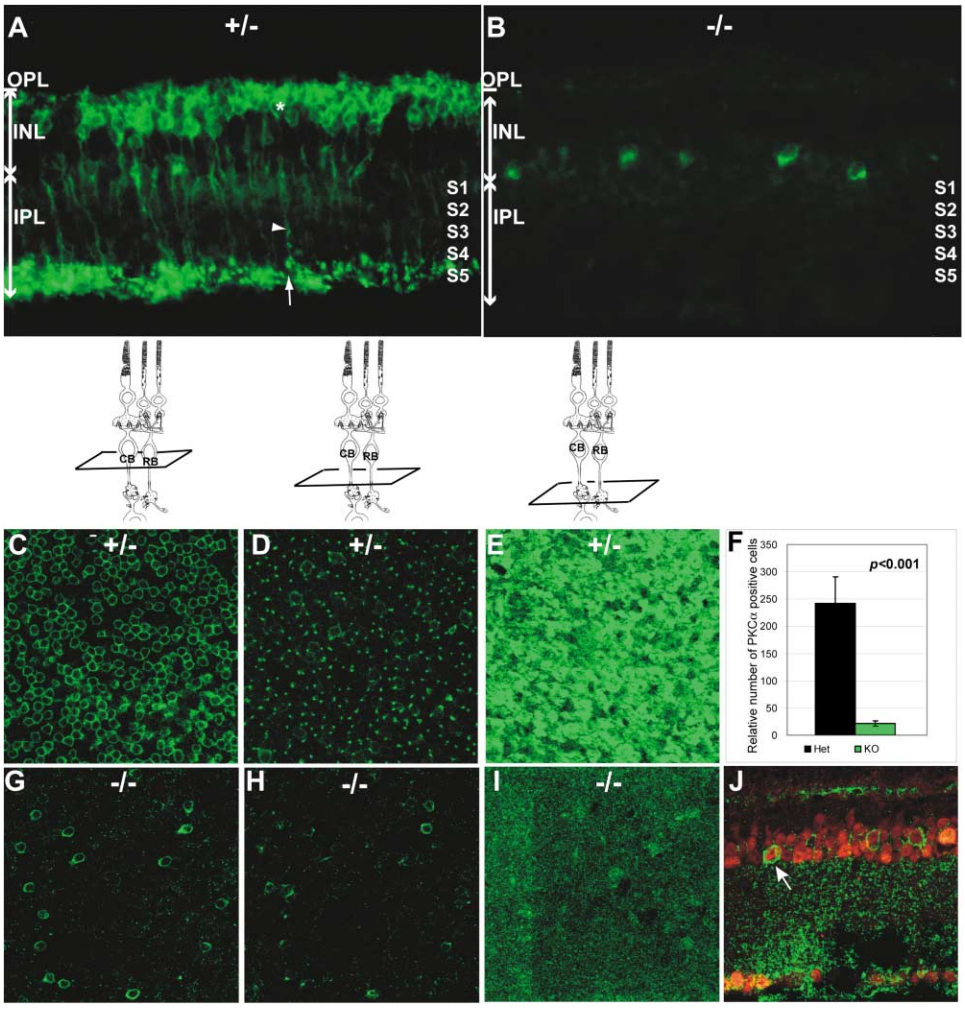


Figure 4. RB Cells Are Missing in the *Bhlhb4* Knockout

Cryosections (20 μm) from adult (3 months) *Bhlhb4*$^{+/-}$ (A) and *Bhlhb4*$^{-/-}$ (B) retinas labeled with anti-PKCα antibodies (green). Asterisk, RB soma; arrowhead, RB axon; arrow, RB terminal. (C–E) *Bhlhb4*$^{+/-}$ and *Bhlhb4*$^{-/-}$ (G–I) retinas from 3-month-old mice labeled with anti-PKCα in whole/flat mount, examined at several different planes of focus. The plane of focus for each pair of images is indicated in the drawings above. (F) The relative difference in PKCα$^{+}$ RB cell number in the *Bhlhb4*$^{-/-}$ and *Bhlhb4*$^{+/-}$ was determined by counting the PKCα$^{+}$ cells per horizontal optical section. Three animals for each genotype were used. (J) Double labeling of a *Bhlhb4*$^{-/-}$ retina with anti-PKCα (green) and the pan-amacrine marker anti-PAX6 (red). Diagrams were modified from Dowling and Boycott (1966). RB, rod bipolar; CB, cone bipolar.

the *Bhlhb4*$^{-/-}$ IPL, corresponding to the processes of the starburst amacrine cell population (Supplemental Figures S1E and S1F).

The AII amacrine cells are essential components of the rod circuitry, serving as the intermediates between RB cells and RGCs. In mice, the AII amacrine cell population strongly expresses the cytoplasmic protein disabled-1 (DAB1), and the loss of *disabled-1* results in a reduced rod b-wave (Rice and Curran, 2000). To determine whether an alteration in the AII amacrine cell population contributed to the loss of b-wave in the *Bhlhb4*$^{-/-}$ mouse, they were labeled with anti-DAB1 antibodies. The number and morphology of cells in the AII population did not appear to be visibly altered in the *Bhlhb4*$^{-/-}$ retina (Supplemental Figures S1G and S1H [http://www.neuron.org/cgi/content/full/43/6/779/DC1]) as compared to the control, although no conclusions can be made regarding the functionality of these cells. Altogether, the loss of *Bhlhb4* affected RB cells and not other neuronal cell types in the INL.

### *Bhlhb4* Is Specifically Expressed in RB Cells

To determine the identity of the cells that normally express *Bhlhb4*, antibodies to β-gal were used to colocalize *Bhlhb4-LacZ* expression with specific INL cell markers. Double IF labeling of *Bhlhb4*$^{+/-}$ retina cryosections with anti-β-gal (Figures 5B and 5C) and anti-PKCα antibodies (Figure 5A) confirmed that *Bhlhb4-LacZ* was expressed in PKCα-expressing cells with RB morphology (Figure 5B). The anti-β-gal labeling was restricted to the upper tier of the INL (Figures 5C and 5F), similar to the observed *LacZ* staining pattern and *Bhlhb4* mRNA expression. *Bhlhb4-LacZ* was also found to be coexpressed with Gοα (Figures 5D–5F), an ON bipolar cell marker (Haverkamp and Wassle, 2000; Vardi, 1998; Vardi et al., 1993), but not with calbindin D, a horizontal cell

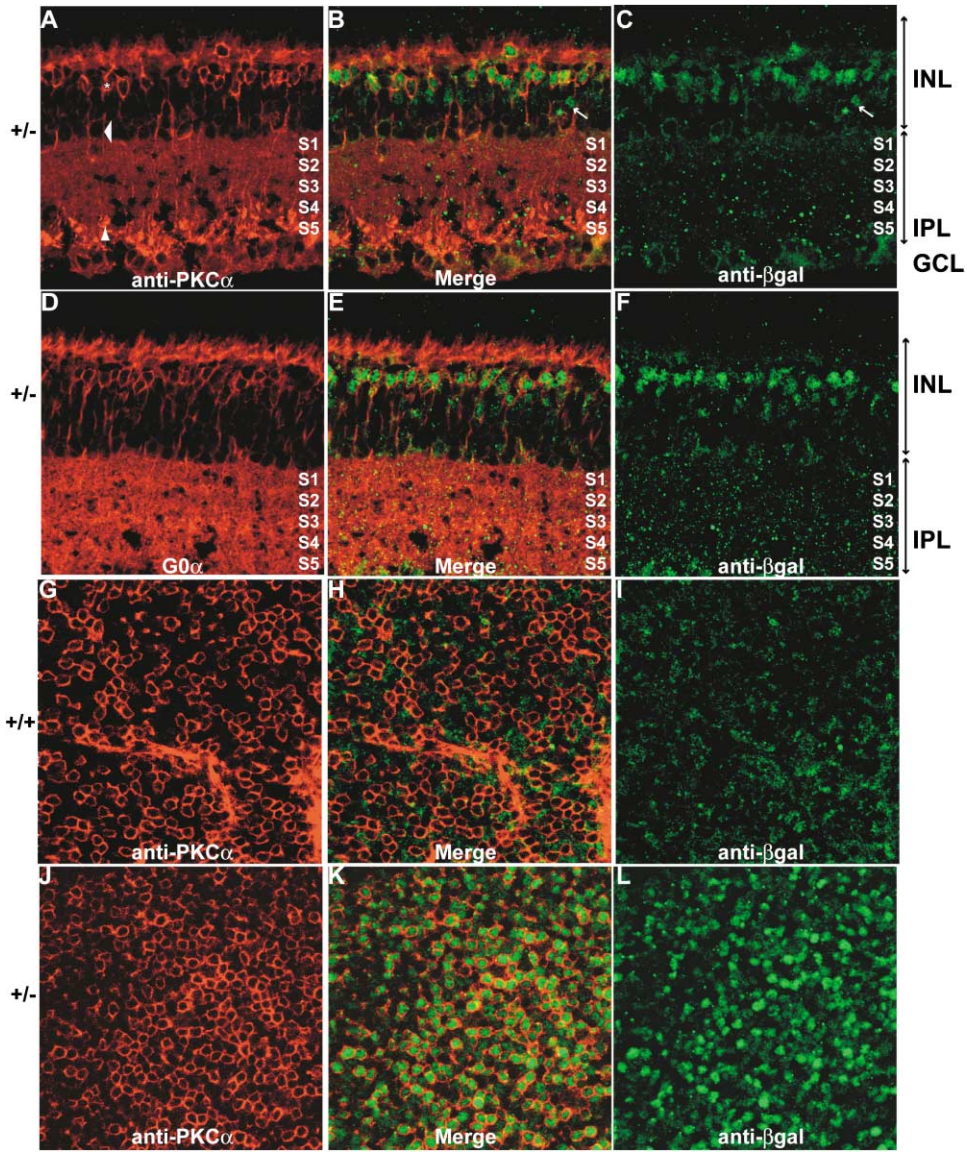


Figure 5. *Bhlhb4* Is Expressed in RB Cells

*Bhlhb4*$^{+/-}$ adult retina cryosections (20 μm), immunolabeled with anti-PKCα (A and B) or anti-G0α (D and E) alone and together with anti-β-gal (green, [B, C, E, and F]). Asterisk, representative RB cell soma; arrowheads, axons; arrows, terminals. One cell, expressing *Bhlhb4-LacZ* but not PKCα, is indicated by the arrow in (B) and (C). Wild-type (G–I) and *Bhlhb4*$^{+/-}$ (J–L) retinas were double immunolabeled in WM with anti-PKCα (red; [G, H, J, and K]) and anti-β-gal (green; [H, I, K, and L]) antibodies. *Bhlhb4-LacZ* is expressed primarily in PKCα-expressing RB cells.

maker (data not shown). A very small number of β-gal$^+$ PKCα$^-$ cells were observed in the *Bhlhb4*$^{+/-}$ retina (Figure 5C, arrow). Triple labeling of *Bhlhb4*$^{+/-}$ retinas with anti-PKCα, anti-G0α, and anti-β-gal antibodies (data not shown) indicated that these cells did not express PKCα nor G0α, suggesting that they may be either an OFF CB subtype or an as yet unidentified cell type.

The colocalization of PKCα and *Bhlhb4-LacZ* expression was confirmed by labeling WM retinas and examining horizontal optical sections (Figures 5G–5L). No cells were labeled by anti-β-gal antibodies in the wt retina (Figures 5H and 5I), while in the heterozygote, all PKCα-expressing RB cells (Figures 5J and 5K) coexpressed *Bhlhb4-LacZ* (Figures 5K and 5L). We cannot rule out the possibility that some RB cells do not express *Bhlhb4*; however, these results showed that nearly 100% of PKCα$^+$ RB cells normally express *Bhlhb4*. None of the PKCα$^+$ amacrine cells, as determined by PAX6 colabeling, morphology, and laminar position, expressed *Bhlhb4-LacZ* (data not shown).

### The Absence of Distinctive RB Cell Terminals and Invaginating Dendritic Processes Confirmed the Loss of the RB Cell Population

The fact that *PKC*α expression was nearly lost in the *Bhlhb4* knockout suggested that the RB cell population

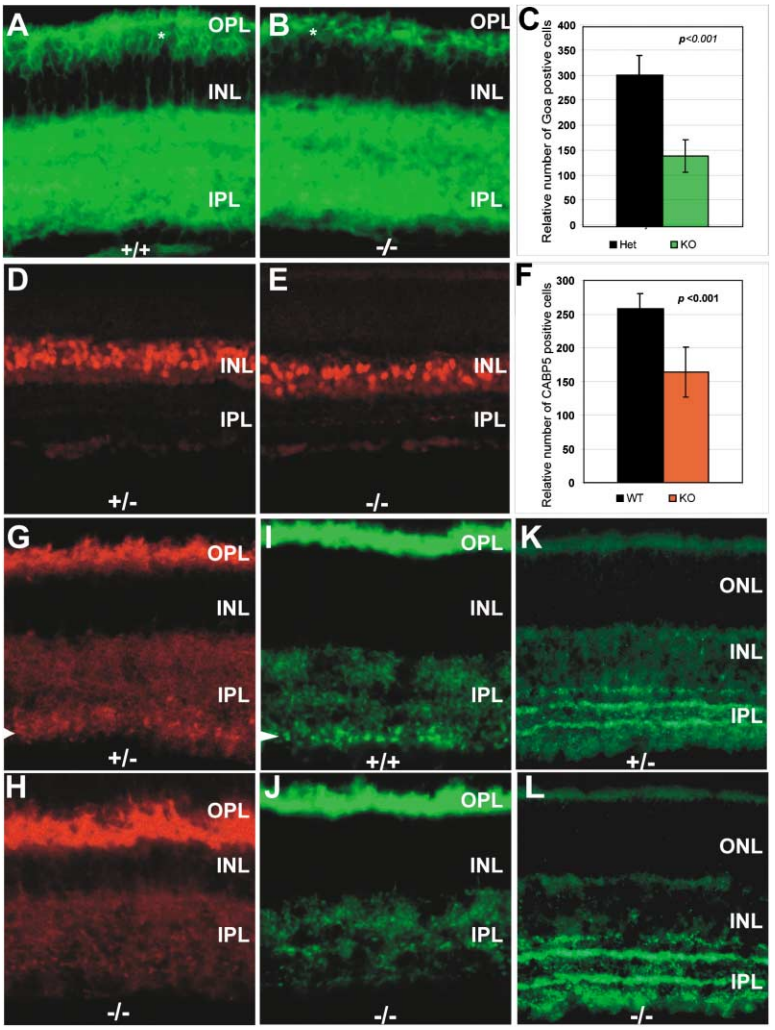


Figure 6. A Reduction in the ON Bipolar Population and Alterations in the Inner Plexiform Layer Supported the Loss of RB Cells in the *Bhlhb4* Knockout

The number of bipolar cells expressing either G0α (A and B) and/or CABP5 (D and E) was reduced in the *Bhlhb4*$^{-/-}$ (B and E) retina. (C and F) Quantification of G0α- or CABP5-expressing cells per optical section of a flat mount retina. Three animals of each genotype were used. The characteristic RB synaptic terminals were strongly labeled by anti-SV2b and vGlut1 in the control IPL (G and I) but were indiscernible in the *Bhlhb4*$^{-/-}$ IPL (H and J). In contrast, SV2b and vGlut1 antibodies strongly labeled the ribbon synapses of photoreceptor terminals in the OPL of both control (G and I) and *Bhlhb4*$^{-/-}$ (H and J) retinas. (K and L) Two tracks of conventional synapses labeled with anti-SV2C antibodies were present in both wt and *Bhlhb4*$^{-/-}$ IPL.

had been abolished. To rule out the possibility that *Bhlhb4* is simply required for PKCα expression in RB cells, several RB cell markers were examined. The number of cells expressing the ON bipolar cell marker G0α was reduced in the *Bhlhb4*$^{-/-}$ retinal sections as compared to controls (Figures 6A and 6B). When the number of G0α-labeled cells in optical sections of retinal flat mounts was counted, the population was decreased by approximately 53% ($p < 0.001$, Student's t test, two-tailed) (Figure 6C and data not shown). Furthermore, the number of cells labeled with *CABP5* (Figures 6D and 6E), which is expressed in RB cells as well as subsets of both ON cone and OFF CB cells (Haverkamp et al., 2003), was reduced by 37% ($p < 0.001$, Student's t test, two-tailed). The reduction in ON bipolar cell numbers is in correlation with the hypothesis that RB cells were lost in the *Bhlhb4*$^{-/-}$ retina.

The loss of RB cells in the *Bhlhb4*$^{-/-}$ retina was further supported by the examination of proteins that play important roles in RB cell dendrites and synaptic terminals in the outer and inner plexiform layers. There are two distinct types of vesicular synapses in the mammalian retina (Sterling, 1998): amacrine cells make conventional synapses, while photoreceptors and bipolar cells form ribbon synapses. Two isoforms of synaptic vesicle protein 2 (SV2) and vesicular glutamate transporter (vGlut1) differentially label synaptic contacts in the retina (Wang et al., 2003). SV2b and vGlut1 are present in the ribbon synapses, while SV2c is present in conventional synapses of starburst amacrine cells in the IPL (Wang et al., 2003). The globular RB cell terminals, distinctive due to their large size and presence in the innermost tier (S5) of the IPL (refer to Figures 4A and 5A), were strongly labeled by anti-SV2b (arrows, Figure 6G) and vGlut1 (Figure 6I) in the wt retina but not the *Bhlhb4* knockout. The synapses weakly labeled by SV2b or vGlut1 in the outer regions of the IPL were observed in both the wt and *Bhlhb4* knockout and likely correspond to the ribbon synapses of the CB cells. These results suggest that RB terminals were missing from the IPL of the *Bhlhb4*$^{-/-}$ retina (Figures 6H and 6J). In contrast, the ribbon synapses of photoreceptor terminals in the OPL are strongly immunolabeled by anti-SV2b (Figures 6G and 6H) and by anti-vGlut1 (Figures 6I and 6J) in the *Bhlhb4* knockout, indicating the integrity of the photoreceptor terminals. In contrast to the anti-SV2b and vGlut1, there was little difference in the anti-SV2c immunolabeling in control and *Bhlhb4*$^{-/-}$ retinas (Figures 6K and 6L), indicating

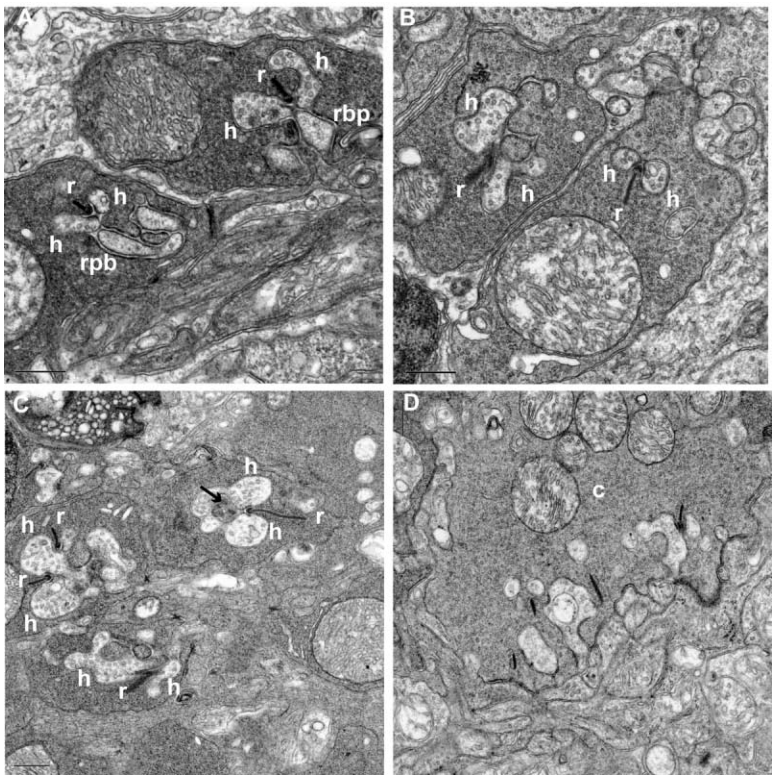


Figure 7. Ultrastructure of the Outer Plexiform Layer

Representative electron micrographs of the retinal OPL (1–3 months) are shown. (A) Synaptic triads in wt OPL with two horizontal cell processes (h) and one RB cell process (rbp) directed toward a ribbon synapse (r) surrounded by tethered vesicles and ended by an electron-dense arch (magnification, 4000×; scale bar, 0.5 μm). (B) Synaptic diads in the *Bhlhb4*$^{-/-}$ OPL with two horizontal cell processes, synaptic ribbons with synaptic vesicles, and electron-dense arch (magnification, 4000×; scale bar, 0.5 μm). (C) Disrupted synaptic structures in the *Bhlhb4*$^{-/-}$ with electron-dense material in place of an RB process (arrow) and very long or multiple ribbons (magnification, 4000×; scale bar, 0.5 μm). (D) A representative cone terminal from the *Bhlhb4*$^{-/-}$ OPL (magnification, 4000×; scale bar, 0.5 μm).

the correct stratification of the IPL by amacrine cell conventional synapses and reiterating the specific effect of the loss of *Bhlhb4* on RB cells.

The integrity of the photoreceptor terminals was examined at the ultrastructural level (Figures 7A–7D). The ribbon synapses formed by rod photoreceptors are in juxtaposition with three dendritic processes, including two horizontal cell processes and one rod-bipolar cell process, that invaginate into the rod terminal forming a synaptic triad (Figure 7A). Comparison of electron micrographs of photoreceptor terminals from wt (Figure 7A) and *Bhlhb4*$^{-/-}$ (Figures 7B and 7C) retina sections at 3 and 6 months (data not shown) revealed that rod (Figures 7B and 7C) and cone (Figure 7D) photoreceptors of the *Bhlhb4*$^{-/-}$ retina form normal ribbon structures. Thus, a disruption of the presynaptic photoreceptor terminal was not likely the cause of the diminished rod b-wave in the *Bhlhb4* knockout. While many synaptic triads were observed in the wt retina (Figure 7A), only a single synaptic triad was observed in all of the *Bhlhb4*$^{-/-}$ photoreceptor terminals examined (Figures 7B and 7C and Table 2). Instead, a significant number of synaptic diads were present in the *Bhlhb4*$^{-/-}$ photoreceptor terminals, indicating the normal synaptogenesis between the rod photoreceptor and horizontal cells but a lack of invaginating RB processes. An increase in the number of unclear, disrupted, or abnormal synaptic junctions in *Bhlhb4*$^{-/-}$ rod terminals, with multiple ribbons and accumulations of dense material at the position of the missing RB process, was also observed (Figure 7C and Table 2). This could have been attempts of the *Bhlhb4*$^{-/-}$ rod photoreceptors to compensate for the loss of RB processes. Increased frequency of rod terminals with multiple synaptic sites has been reported to occur in the degenerating retina (Jansen et al., 1997). In contrast, the cone terminals were similar in *Bhlhb4*$^{-/-}$ and wt retinas (Figure 7D and data not shown). The ultrastructural analysis at the level of the OPL showed that rod photoreceptor terminals developed normally and confirmed that RB cell processes are missing in the adult *Bhlhb4* knockout.

### Failure of RB Cell Maturation to Progress in *Bhlhb4*$^{-/-}$ Mice

In the *Bhlhb4* knockout, PKCα$^{+}$ RB cells may have failed to differentiate or they may have been progressively lost over time such that they were undetectable in the adult *Bhlhb4* knockout. Thus, anti-PKCα labeling was examined during development. *Bhlhb4*$^{-/-}$ and wt retinal tissue was harvested at several time points in the postnatal retinal development (P6–P14), and the P8 results are shown. In the wt mouse, PKCα$^{+}$ cells can be detected in both the wt and *Bhlhb4*$^{-/-}$ retina as early at P6 (Wang et al., 2003, and data not shown), but the alignment of RB cell terminals at the innermost level of the IPL is generally not detected in the mouse retina until P8 (Figures 8A and 8B) (Wang et al., 2003). Surprisingly, significant numbers of PKCα-expressing RB cells were found in the P8 *Bhlhb4*$^{-/-}$ retinas (Figures 8D–8F and 8H). These presumptive *Bhlhb4*$^{-/-}$ RB cells appeared to be able to mature to the point that they expressed RB cell type-specific markers, aligned themselves at the outer edge of the INL, and extended axonal processes, similar to the wt littermate (Figures 8A–8C). At P8, the PKCα$^{+}$ RB cells in both the wt littermate and the *Bhlhb4* knockout coexpressed the ON bipolar marker Gοα (Figures 8B and 8C and 8E and 8F). *Bhlhb4-LacZ* and PKCα

Table 2. Quantification of Synaptic Diads and Triads in the OPL

| | Number of Triads | Number of Diads | Multiple Ribbons | Ribbon Unclear | Terminals with Ribbon | Terminals without a Ribbon |
|---|---|---|---|---|---|---|
| Wild-type | 58 (40.3%) | 40 (27.8%) | 4 (2.8%) | 42 (29.2%) | 144 | 59 |
| *Bhlhb4*$^{-/-}$ | 1 (0.8%) | 76 (60.3%) | 9 (7.1%) | 40 (31.7%) | 127 | 89 |

Retinas derived from three animals in each genotype group. A total of 56 electron micrographs of *Bhlhb4*$^{-/-}$ retinas and 65 micrographs of wild-type taken at 4000× were counted. Terminals with multiple ribbons or with unclear synaptic structures were counted separately. Percentages of the total number of terminals with ribbons are in parentheses. Terminals without ribbons or unclear structures reflected the variation of angle/position of the sections through each terminal.

colocalization was detected in both *Bhlhb4*$^{+/-}$ and *Bhlhb4*$^{-/-}$ retinas at P8 (Figures 8G and 8H).

At P8, the number of PKC$\alpha$ cells was already reduced by 64.7% ($p < 0.001$, Student's t test, two-tailed), and the projection of axons and formation of terminals was markedly reduced (Figure 8D). However, the cell loss in the *Bhlhb4* knockout was progressive in that the percent reduction in RB cells increased from 64.7% at P8 to 91.2% in the 2- to 3-month-old animals, and the relative number of RB cells present at P8 in the *Bhlhb4*$^{-/-}$ was significantly more than in the 2- to 3-month-old animals ($p < 0.001$, Student's t test, two-tailed) (Figure 8K). The loss of RB cell terminals, axons, and somata progressed quickly such that only a few PKC$\alpha$-labeled somata could be detected in the *Bhlhb4*$^{-/-}$ by P12 and no axons could be detected (data not shown).

The presence of a significant number of PKC$\alpha$-expressing cells in the P8 *Bhlhb4*$^{-/-}$ retina and the progressive loss of these cells during retinal maturation eliminated the possibility that RB cells fail to be born. Furthermore, examination of the overall number of proliferating cells during early postnatal retinal development (P1–P6) in *Bhlhb4*$^{-/-}$ and wt control retinas by monitoring BrdU incorporation (Figure 8 and data not shown) demonstrated similar levels of proliferation in the wt and *Bhlhb4*$^{-/-}$ animal. Furthermore, proliferation in the central retina was complete by P5, although some BrdU-labeled cells were found at the retinal periphery (data not shown). This is in contrast to *Bhlhb4* expression, which is first observed in the central retina at P5 (Figure 1I) and is not expressed in the peripheral aspects of the retina until P8 when all proliferation had ceased.

The rate of cell death in *Bhlhb4*$^{-/-}$ retinas as compared to controls was examined by using cleaved-caspase-3, an early marker for apoptosis. An increase in the number of apoptotic cells in the INL was observed in the *Bhlhb4* knockout between P8 and P10 (Figures 8L–8P), while, at earlier and later stages, the number of apoptotic cells did not appear to be significantly different (data not shown). Cell death does play an important role in normal retinal development, and the degeneration of bipolar and Müller cells normally reaches a peak between P8 and P11 (Young, 1984). However, the rate of apoptosis was aproximately 45% greater at P8 ($p < 0.001$, Student's t test, two-tailed) and 32% greater at P10 ($p < 0.01$, Student's t test, two-tailed) in *Bhlhb4*$^{-/-}$ retinas than controls (Figure 8P). The increase at P8 and P10 and not at P6 was confirmed by FragEL DNA fragmentation detection assays on adjacent sections (data not shown). In addition, apoptotic cells colabeled with anti-PKC$\alpha$ and anti-cleaved-caspase-3 antibodies were detected at P8 and P10 (data not shown). These data suggested that RB cells in the *Bhlhb4* knockout underwent apoptosis beginning around P8 such that the population was nearly depleted by P12.

## Discussion

The RB population did not recover in the mature *Bhlhb4*$^{-/-}$ retina, accounting for the dramatic loss of ERG b-wave of the adult *Bhlhb4*$^{-/-}$ mouse. ERG recordings displayed a dramatic reduction in the scotopic b-wave elicited from RB cells but sustained a normal a-wave derived from the photoreceptor population, indicating the lack of dependence of the rod photoreceptor population on the RB targets. The residual rod b-wave at observed higher intensities in the *Bhlhb4* knockout could represent a diminished response from residual RB cells. However, since the highest intensities are above the cone threshold, this residual b-wave likely represents a contribution from CB cells. Alternatively, this may be a manifestation of a coupling between rods and cones said to exist through gap junctions, providing an alternative route for scotopic transmission to the inner retina (Bloomfield and Dacheux, 2001), and should be investigated further.

*Bhlhb4* expression was restricted to PKC$\alpha^+$ RB cells, which were nearly abolished in the adult *Bhlhb4* knockout, accounting for the dramatic loss of retinal activity. However, *Bhlhb4* may also be expressed in other cells in the retina. Some cells positive for *Bhlhb4-LacZ* expression in the *Bhlhb4*$^{+/-}$ retina did not coexpress PKC$\alpha$ (Figures 5B and 5C, arrow), indicating that *Bhlhb4* is expressed in one or more other cell types in the INL in addition to RB cells. $\beta$-gal$^+$/PKC$\alpha^-$ cells were also observed in the *Bhlhb4*$^{-/-}$ retina (data not shown). The $\beta$-gal$^+$/PKC$\alpha^-$ cells observed in the *Bhlhb4*$^{+/-}$ retina and those remaining in the *Bhlhb4*$^{-/-}$ retina have yet to be identified. However, they appear to be a bipolar cell type expressing Chx10 (data not shown) and not the pan-amacrine cell marker Pax6. These cells do not express PKC$\alpha$ or G0$\alpha$ (ON bipolar), caldendrin (OFF CB), calretinin (starburst amacrine), or calbindin D (horizontal cells). Thus, *Bhlhb4* appears to be expressed in an as yet unidentified INL cell type.

Further investigation into the *Bhlhb4*$^{-/-}$ phenotype revealed that RB cells were born but failed to survive neuronal maturation. Thus, during development, *Bhlhb4* functions downstream of those factors that together dictate bipolar cell specification (Chx10, Mash1, and Math3) and contributes to the RB cell subtype identity and function. The depletion of RB cells was concurrent

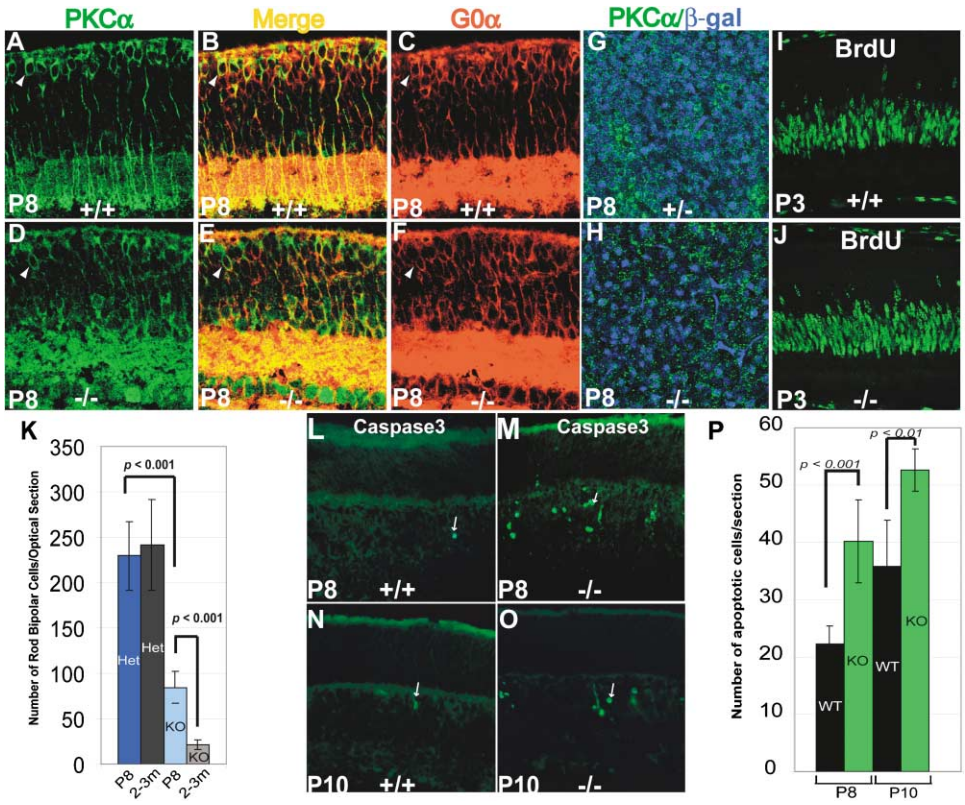


Figure 8. Postnatal Development of the RB Cell Population

Retinal tissue from P8 *Bhlhb4*$^{-/-}$ (A–C) and wt mice (D–F) labeled with anti-PKCα (A, B, D, and E) and anti-G0α (B, C, E, and F) antibodies. PKCα-expressing RB cell somata aligned at the outer edge of the INL were observed in both wt (+/+) and *Bhlhb4*$^{-/-}$ (−/−) retinas at P8. PKCα and G0α colocalization (yellow) was observed in RB cells of wt (B) and *Bhlhb4*$^{-/-}$ (E) animals. Arrowheads show representative RB cells coexpressing PKCα and G0α. (G and H) Optical sections at the level of the INL of P8 wt (G) and P8 *Bhlhb4*$^{-/-}$ (H) WM retinas labeled with anti-PKCα (green) and anti-β-gal antibodies (blue). (I and J) BrdU incorporation in P3 wt (I) and *Bhlhb4*$^{-/-}$ (J) retinas. (K) Quantification of PKCα$^{+}$ RB cells in optical sections of WM P8 retina as compared to 2- to 3-month-old adult retina . (L–O) Anti-cleaved-caspase-3 labeling of wt (L and N) and *Bhlhb4*$^{-/-}$ (M and O) retinal sections at P8 and P10. (P) Quantification of the total number of apoptotic cells/section.

with the peak of *Bhlhb4* expression at P8 (Figures 1I–1R) and coincided with several key events in RB the maturation. RB cell terminals are aligned in the innermost tier of the IPL by P8, when *Bhlhb4* expression is at its peak. Two days later, at P10, RB cell dendrites invade rod terminals to establish the first rod triads and the first ribbon synapses are said to appear in the RB terminals (Sherry et al., 2003). The timing of these events corresponds to the significant increase in INL cell apoptosis in the *Bhlhb4*$^{-/-}$ retina, supporting the hypothesis that the loss of *Bhlhb4* precludes RB cell maturation and leads to cell death.

Whether the dendritic processes of *Bhlhb4*$^{-/-}$ RB cells would have been capable of invading the rod terminals or forming functional synapses had they survived or whether the RB cells died due to a failure to form functional contacts with pre- or postsynaptic cell types is not clear at this time. However, it is striking that the increased cell death in the *Bhlhb4* knockout occurs at P8 at a time when the final stages of neuronal maturation are underway in the RB cell population, as the dependence of inner retinal neuron survival on the integrity of the photoreceptor population has been reported (Strettoi and Pignatelli, 2000; Marc et al., 2003; Leconte and Barnstable, 2000). The survival of developing neurons is dependent upon trophic factors and the proper formation of contacts with neighboring cells and target cells (Putcha et al., 2000). Therefore, it is tempting to propose that developing RB cells succumb to cell death in the *Bhlhb4*$^{-/-}$ mice as a consequence of their inability to form functional contacts with the photoreceptors during a critical window in time. Alternatively, the *Bhlhb4*$^{-/-}$ RB cell population could have succumbed to cell death due to poor synaptogenesis with target cells.

There are other mouse mutants that exhibit a lack of an ERG b-wave, such as the reeler mouse and the scrambler mouse that have mutations in the *reelin* and *disabled* (*DAB1*) genes, respectively. *DAB1* is expressed in the INL and strongly in AII amacrine cells, while *reelin* is expressed in the GCL and in lamina b of the IPL as well as in bipolar cells and amacrine cells of the INL. Reduced b-waves in both of these mutant mouse strains indicate that the reelin pathway contributes to rod-driven retinal responses (Rice et al., 2001; Rice and Curran, 2000). The diminished ERG b-wave was attributed to an insufficient number of RB cells to provide synaptic input to type AII amacrine cells in mice lacking either *reelin* or *DAB1*, although neither gene is ex-

pressed in RB cells. The reduction in RB cells in the reeler and disabled mouse strains was reported to occur later in postnatal development (P12), at a time corresponding to RB cell functional maturation, from displaying ribbon synapses to expressing *vGlut1* (Sherry et al., 2003). It was suggested that disruption in the *reelin* pathway caused a deficiency in the AII amacrine cell dendritic arborization, depriving a subset of RB axons of trophic factors that are critical for survival at a time when synaptic connections are being made (Rice et al., 2001). Although we have not identified any amacrine cell abnormality in the *Bhlhb4* knockout, it is possible that *Bhlhb4*$^{-/-}$ RB cell survival depends on a reciprocal interaction with amacrine cells and RB cells at a critical time point.

The intracellular signaling pathways that are integral to the RB cell-mediated transmission of light information are largely unknown. Analysis of murine loss-of-function mutants has revealed key proteins that are required for the ON bipolar cell response. The metabotropic glutamate receptor *mGluR6* is expressed in ON bipolar cells, and the loss of *mGluR6* in the mouse blocks the ON response to changes in glutamate release from photoreceptors, abolishing the ERG b-wave (Masu et al., 1995). The trimeric G protein G0$\alpha$ is believed to be the second step in the ON bipolar cell signaling cascade descending from *mGluR6* (Vardi, 1998; Dhingra et al., 2000; Nawy, 1999). Deletion of the GO$\alpha$ gene results in the complete absence of the ON response (ERG b-wave) (Dhingra et al., 2000).

The genetic ablation of *mGluR6* or *GO*$\alpha$ results in no abnormality in the cell number or the morphology of the RB population (Tagawa et al., 1999; Dhingra et al., 2000). This opposes the idea that *Bhlhb4*$^{-/-}$ RB cell death is due to a loss of activity, and one might propose that RB cell survival is not activity dependent. Alternatively, other non-mGluR6-mediated contacts with neighboring retinal neurons, which are affected by the loss of *Bhlhb4*, may be sufficient for RB survival in the absence of *mGluR6*. In either case, further study of *Bhlhb4* will lead to the identification of factors that are necessary for RB survival, and these are likely to be essential for cellular interactions.

The *Bhlhb4*$^{-/-}$ phenotype—a dramatic reduction in scotopic b-wave—is commonly referred to as "negative ERG." In humans, negative ERG is often associated with a condition referred to as congenital stationary night blindness (CSNB) (Dryja, 2000). CSNB is most often an X-linked trait, while *Bhlhb4* is localized to the distal end of human chromosome 20 (Bramblett et al., 2002), excluding it as the determinate of X-linked CSNB. However, *Bhlhb4* may influence the RB pathway(s) disrupted in CSNB, as autosomal-dominant and -recessive forms of CSNB do occur (Dryja, 2000; Fitzgerald et al., 2001). Thus, the *Bhlhb4* knockout can be considered a mouse model for CSNB-like conditions, as all are characterized by a deficiency in the rod component of the retinal response to light.

The genes that are responsible for the two forms of X-linked CSNB, incomplete and complete, have been identified. Bipolar cells convey information changes in their membrane potential and modulate transmitter release through the influx of calcium via L-type calcium channels (Berntson et al., 2003), and a mutation in the gene CACNA1F, which encodes the $\alpha$-1 subunit of an L-type calcium channel in mouse and humans (Bech-Hansen et al., 1998; Strom et al., 1998), is responsible for incomplete CSNB. The no b-wave (NOB) mouse displays the complete form of the X-linked CSNB phenotype (Pardue et al., 1998). The defective gene responsible for the NOB phenotype in mice and the complete CSNB form in humans is the gene nyctalopin (*Nyc*) (Bech-Hansen et al., 2000; Pusch et al., 2000; Gregg et al., 2003). Nyc is a membrane-anchored extracellular protein that is expressed in the cells of the INL and the GCL, but no function has been associated with Nyc. Although both are required for RB cell function, neither *Nyc* nor CAC NA1F mutations have been related to RB cell survival (Ball et al., 2003). Still, it is possible that *Bhlhb4* is involved in the same functional pathway(s) as Nyc and/or CACNA1F in adult RB cells, but only after it has mediated events that support RB cell maturation and survival during development.

The survival of maturing neurons depends upon trophic factors and the formation of functional contacts with neighboring cells and target cells. The identification of *Bhlhb4* has opened the door to the discovery of genes that are required for neuronal maturation. Given the timing of *Bhlhb4* expression, its correlation with both the depletion of the RB population in the *Bhlhb4* knockout and with normal RB cell maturation in the wt animal, we predict that, as a transcriptional regulator, *Bhlhb4* regulates genes that are key to RB synaptogenesis and/or signal transmission. Hopefully, further study of the *Bhlhb4*$^{-/-}$ model will further the understanding of RB intracellular signaling and the etiology of diseases that impact the rod circuitry, such as CSNB.

## Experimental Procedures

### Targeting Construct

Genomic sequences homologous to the *Bhlhb4* locus were used to flank an IRES-LacZ/Pgk-NeoLoxP cassette (a gift from Dr. Richard Behringer, M.D. Anderson), allowing for specific targeting of the *Bhlhb4* locus by homologous recombination. A 20 kb genomic fragment containing the entire *Bhlhb4* gene was isolated from a Lambda gtII phage, 129Sv mouse genomic library (a kind gift from P. Soriano, University of Washington, Seattle, WA). The 5′ arm of the final targeting construct is 4.3 kb in length and extends downstream to the naturally occurring SfiI restriction site located upstream of the first ATG in the open reading frame. The 3′ arm is a 2.5 kb XbaI/EcoRI genomic fragment that begins immediately upstream of the *Bhlhb4* stop codon.

### ES Cell Culture and Blastocyst Injections

The targeting construct, linearized with a unique NotI site located immediately upstream of the 5′ flanking sequence, was introduced into 129SvEv AB2.1 embryonic stem cells (ES) by electroporation. Transfected ES cells were grown on $\gamma$-irradiated STO feeder cells in ES cell media under selective conditions (G418). Homologous recombination in ES cell clones at the *Bhlhb4* locus was confirmed by Southern blot using the probe a (Figures 1A–1C). Multiple/random integrations were identified and excluded by Southern blot using a probe to neomycin (NEO). Correctly targeted ES cells from single clones were microinjected into C57Bl6 blastocysts, and chimeric blastocysts were used to generate chimeric offspring. Chimeric male mice with high ES cell contribution (95%) (as judged by coat color) were bred to C57Bl6 females to derive heterozygous *Bhlhb4* mutant (*Bhlhb4*$^{+/-}$) mice. The resultant *Bhlhb4*$^{+/-}$ mice with 129svev/C57Bl6 background were backcrossed to C57Bl6 for seven generations (F7). *Bhlhb4*$^{-/-}$ mice were generated by heterozygous matings.

### Genotyping

The animal genotypes were determined by three primer PCR. Each PCR reaction contained 20 pmol of each primer (P1, 5′- ATCTTC AGGCCCGTGGGTCC; P2, 5′-AGGCCTGCGCCTGCATGAG; P3, 5′-GACATTCAACAGACCTTGCATTCC), 0.4 mM dXTP, 2 mM $MgCl_2$, 5% DMSO (v/v), 2.5 units Taq DNA Polmerase (Gene Choice) in 1× Gene Choice reaction buffer. The primer pair P1 and P2 amplify a 683 bp fragment from the wt allele (Figures 1A, 1B, and 1D). The primer pair P1 and P3 amplify a 468 bp fragment spanning the 5′ junction between the 5′ arm and the IRES-LACZ insertion of the mutant allele.

### LacZ Staining

For adult tissues, animals were deeply anesthetized with 0.02 ml/gr body weight 2.5% Avertin and then were perfused with PBS pH7.3/Heparin followed by a solution of 2% paraformaldehyde, 2 mM $MgCl_2$, 5 mM EGTA. Eyes were then subjected to LacZ staining as described previously (Pennesi et al., 2003).

### In Situ Hybridization

Radioactive in situ hybridizations were performed on 7 μm paraffin sections as described previously (Bramblett et al., 2002). Nonradioactive in situ hybridizations on 20 μm cryosections were performed using Digoxygenin (Dig)-labeled RNA probes synthesized using a 1.5 kb *Bhlhb4* cDNA subfragment (pbks-Beta4,1.5) as the template. Hybridization and washing steps were performed as described for radioactive hybridization. Following hybridization, sections were incubated with anti-Dig-alkaline phosphatase (AP) antibodies (Roche) in 1% Roche blocking reagent plus 5% normal serum overnight. Sections were then washed in Tris-buffered saline plus 1% Tween-20 ([TBST], 0.14 M NaCl, 0.27 mM KCL, 25 mM Tris, pH 7.5, 1% Tween-20). The AP activity was detected using a mixture of BCIP (5-bromo-4-chloro-3-indolyl phosphate) and NBT (p-nitroblue tetrazolium chloride) (Roche) in Tris-buffered saline plus magnesium-chloride and 1% Tween-20 ([NTMT], 100 mM NaCl, 100 mMTris, pH 9.5, 50 mM $MgCl_2$, and 1% Tween-20).

### Immunofluorescent Labeling

Tissues were prepared for IF labeling according to procedures described elsewhere (Haverkamp and Wassle, 2000). Sections were blocked in a solution of 5% BSA, 1% cold water fish skin gelatin (CWFS) (Electron Microscopy Sciences, Washington, PA), 10% normal serum in PBS (pH 7.4) for 1 hr at room temperature. Following blocking, the sections were incubated with primary antibodies in blocking buffer for 18–36 hr at 4°C. Sections were then washed three times, incubated with biotin-SP-conjugated AffiniPure $F(ab')_2$ fragment donkey anti-species antibodies (Jackson ImmunoResearch Inc., West Grove, PA) in blocking buffer for 30 min, washed three times, incubated with fluorophore-conjugated streptavidin (Molecular Probes, Eugene, OR) for 30 min, and washed three to five times for 10 min with PBS. Slides were prepared for viewing with ProLong mounting medium (Molecular Probes). Sections labeled with a single antibody or in brightfield were visualized using a Zeiss Axioskop2 microscope outfitted with a Zeiss AxioCam MRC digital video camera. For retinas immunolabeled in whole mount (WM), the blocking buffer was altered to include (0.5% Triton X-100), blocking was increased to 18–24 hr, primary and secondary antibody incubations were increased to 72 hr, and washing steps were increased to five or six times for 1 hr. The WM retinas were mounted flat GCL face up on slides with prolong mounting media. WM retinas and double immunolabeled cryosections were visualized using a Zeiss LSM 510 META Confocal/Spectral Imaging microscope. For BrdU labeling, pups were injected with 0.1 ml BrdU labeling solution (Amersham, RPN201V1) per gram body weight, and the tissue was harvested after 30 min. Brdu incorporation was detected using the Amersham anti-BrdU antibody (Amersham, RPN202), biotinylated anti-mouse plus Cy2-streptavidin.

The following antibodies were used for IF labeling: goat anti-β-galactosidase (4600-1409, Biogenesis, England, UK) at 1:200; mouse anti-calbindin D (C8666, Sigma, St. Louis, MO) at 1:400; rabbit anti-calretinin (AB149Chemicon, Temecula, CA) at 1:1000; rabbit anti-CABP5 (UW89, Yoshikazu Imanishi, University of Washington) at 1:400; guinea pig anti-caldendrin (Cortico GbR, Magedeburg, Germany) at 1:300; rabbit anti-caspase-3 (Asp175) (Cell Signaling Technology) at 1:500; rabbit anti-DAB1 (100-401-225 Rockland, Gilbertsville, PA) at 1:1000; mouse anti-Gοα (MAB3073, Chemicon, Temecula ,CA) at 1:500; guinea pig anti-VGlut1 (AB5905, Chemicon) at 1:1000; rabbit anti-Pax6 (AB5409, Chemicon) at 1:1000; rabbit anti- PKCα (#PK 14, Oxford Biomedical Research) at 1:500; mouse anti-PKCa (610107, BD Transduction Labs) at 1:500; rabbit anti-SV2b and SV2c (Roger Janz, UT- Houston Medical School) at 1:500.

### Electroretinograms

One- to two-month-old mice of both sexes were used for the ERGs. For the scotopic ERGs, mice were allowed to adapt to the dark overnight. Under dim red light, mice were anesthetized with a solution of ketamine (95 mg/ml) and xylazine (5 mg/ml). The pupils were then dilated with a single drop of 0.5% mydryacil and 2.5% phenylephrine. A drop of 0.5% proparacaine dydropcholride was applied for corneal anesthesia. Electroretinograms were conducted and analyzed by the methods described previously (Pennesi et al., 2003a, 2003b).

### Transmission Electron Microscopy

Retina samples isolated from four animals of each genotype were prepared by dissecting cornea and lenses away from the eye cups while in fixative (2.5% glutaraldehyde in 0.1 M cacodylate buffer with 2 mM $CaCl_2$). Tissues were then prepared for transmission electron microscopy (TEM) in flat mount as described previously (Mancini et al., 1986). Sections 500 nm thick were cut using the RMC MT6000 ultramicrotome and were counterstained with Toluidine blue. Subsequently, thin sections of 60 nm were cut and stained with 2% alcoholic uranyl acetate and Reynold's lead citrate. Grids were viewed on Hitachi-H7500 TEM. Digital images were acquired using a Gatan 2kx2k CCD camera.

### Acknowledgments

We would like to thank Francesco DeMayo and the BCM Transgenic Mouse Core for assistance with embryo manipulations; Claire Haueter for TEM assistance; Sophia Tsai, Fred Pereira, Jang-Hyeon Cho, and Khoi Chu for helpful discussion and/or editorial comments; Dr. Roger Janz for the Sv2 antibodies; and Dr. Yoshikazy Imanishi for anti-CABP5. Funding from the NIDDK (to D.E.B.), NIH (to M.-J.T.), NIH EY04446 and EY02520, the Retina Research Foundation (Houston), the International Retinal Research Foundation, Inc., and Research to Prevent Blindness (to S.M.W.) supported this work.

Received: April 9, 2004
Revised: July 27, 2004
Accepted: August 19, 2004
Published: September 15, 2004

### References

Akagi, T., Inoue, T., Miyoshi, G., Bessho, Y., Takahashi, M., Lee, J.E., Guillemot, F., and Kageyama, R. (2004). Requirement of multiple basic helix-loop-helix genes for retinal neuronal subtype specification. J. Biol. Chem. *279*, 28492–28498.

Ball, S.L., Pardue, M.T., McCall, M.A., Gregg, R.G., and Peachey, N.S. (2003). Immunohistochemical analysis of the outer plexiform layer in the nob mouse shows no abnormalities. Vis. Neurosci. *20*, 267–272.

Bech-Hansen, N.T., Boycott, K.M., Gratton, K.J., Ross, D.A., Field, L.L., and Pearce, W.G. (1998). Localization of a gene for incomplete X-linked congenital stationary night blindness to the interval between DXS6849 and DXS8023 in Xp11.23. Hum. Genet. *103*, 124–130.

Bech-Hansen, N.T., Naylor, M.J., Maybaum, T.A., Sparkes, R.L., Koop, B., Birch, D.G., Bergen, A.A., Prinsen, C.F., Polomeno, R.C., Gal, A., et al. (2000). Mutations in NYX, encoding the leucine-rich proteoglycan nyctalopin, cause X-linked complete congenital stationary night blindness. Nat. Genet. *26*, 319–323.

Berntson, A., Taylor, W.R., and Morgans, C.W. (2003). Molecular

identity, synaptic localization, and physiology of calcium channels in retinal bipolar cells. J. Neurosci. Res. *71*, 146–151.

Bloomfield, S.A., and Dacheux, R.F. (2001). Rod vision: pathways and processing in the mammalian retina. Prog. Retin. Eye Res. *20*, 351–384.

Bramblett, D.E., Copeland, N.G., Jenkins, N.A., and Tsai, M.J. (2002). BHLHB4 is a bHLH transcriptional regulator in pancreas and brain that marks the dimesencephalic boundary. Genomics *79*, 402–412.

Burmeister, M., Novak, J., Liang, M.Y., Basu, S., Ploder, L., Hawes, N.L., Vidgen, D., Hoover, F., Goldman, D., Kalnins, V.I., et al. (1996). Ocular retardation mouse caused by Chx10 homeobox null allele: impaired retinal progenitor proliferation and bipolar cell differentiation. Nat. Genet. *12*, 376–384.

Cepko, C.L., Austin, C.P., Yang, X., Alexiades, M., and Ezzeddine, D. (1996). Cell fate determination in the vertebrate retina. Proc. Natl. Acad. Sci. USA *93*, 589–595.

De Melo, J., Qiu, X., Du, G., Cristante, L., and Eisenstat, D.D. (2003). Dlx1, Dlx2, Pax6, Brn3b, and Chx10 homeobox gene expression defines the retinal ganglion and inner nuclear layers of the developing and adult mouse retina. J. Comp. Neurol. *461*, 187–204.

Dhingra, A., Lyubarsky, A., Jiang, M., Pugh, E.N., Jr., Birnbaumer, L., Sterling, P., and Vardi, N. (2000). The light response of ON bipolar neurons requires G[alpha]o. J. Neurosci. *20*, 9053–9058.

Dowling, J.E., and Boycott, B.B. (1966). Organization of the primate retina: electron microscopy. Proc. R. Soc. Lond. B. Biol. Sci. *166*, 80–111.

Dryja, T.P. (2000). Molecular genetics of Oguchi disease, fundus albipunctatus, and other forms of stationary night blindness. LVII Edward Jackson Memorial Lecture. Am. J. Ophthalmol. *130*, 547–563.

Fitzgerald, K.M., Hashimoto, T., Hug, T.E., Cibis, G.W., and Harris, D.J. (2001). Autosomal dominant inheritance of a negative electroretinogram phenotype in three generations. Am. J. Ophthalmol. *131*, 495–502.

Ghosh, K.K., Bujan, S., Haverkamp, S., Feigenspan, A., and Wassle, H. (2004). Types of bipolar cells in the mouse retina. J. Comp. Neurol. *469*, 70–82.

Gregg, R.G., Mukhopadhyay, S., Candille, S.I., Ball, S.L., Pardue, M.T., McCall, M.A., and Peachey, N.S. (2003). Identification of the gene and the mutation responsible for the mouse nob phenotype. Invest. Ophthalmol. Vis. Sci. *44*, 378–384.

Hatakeyama, J., Tomita, K., Inoue, T., and Kageyama, R. (2001). Roles of homeobox and bHLH genes in specification of a retinal cell type. Development *128*, 1313–1322.

Haverkamp, S.F., and Wassle, H. (2000). Immunocytochemical analysis of the mouse retina. J. Comp. Neurol. *424*, 1–23.

Haverkamp, S., Ghosh, K.K., Hirano, A.A., and Wassle, H. (2003). Immunocytochemical description of five bipolar cell types of the mouse retina. J. Comp. Neurol. *455*, 463–476.

Hood, D.C., and Birch, D.G. (1994). Rod phototransduction in retinitis pigmentosa: estimation and interpretation of parameters derived from the rod a-wave. Invest. Ophthalmol. Vis. Sci. *35*, 2948–2961.

Jansen, H.G., Hawkins, R.K., and Sanyal, S. (1997). Synaptic growth in the rod terminals of mice after partial photoreceptor cell loss: a three-dimensional ultrastructural study. Microsc. Res. Tech. *36*, 96–105.

Leconte, L., and Barnstable, C.J. (2000). Impairment of rod cGMP-gated channel alpha-subunit expression leads to photoreceptor and bipolar cell degeneration. Invest. Ophthalmol. Vis. Sci. *41*, 917–926.

Liu, I.S., Chen, J.D., Ploder, L., Vidgen, D., van der Kooy, D., Kalnins, V.I., and McInnes, R.R. (1994). Developmental expression of a novel murine homeobox gene (Chx10): evidence for roles in determination of the neuroretina and inner nuclear layer. Neuron *13*, 377–393.

Mancini, M.A., Frank, R.N., Keirn, R.J., Kennedy, A., and Khoury, J.K. (1986). Does the retinal pigment epithelium polarize the choriocapillaris? Invest. Ophthalmol. Vis. Sci. *27*, 336–345.

Marc, R.E., Jones, B.W., Watt, C.B., and Strettoi, E. (2003). Neural remodeling in retinal degeneration. Prog. Retin. Eye Res. *22*, 607–655.

Masu, M., Iwakabe, H., Tagawa, Y., Miyoshi, T., Yamashita, M., Fukuda, Y., Sasaki, H., Hiroi, K., Nakamura, Y., and Shigemoto, R. (1995). Specific deficit of the ON response in visual transmission by targeted disruption of the mGluR6 gene. Cell *80*, 757–765.

Nawy, S. (1999). The metabotropic receptor mGluR6 may signal through G(o), but not phosphodiesterase, in retinal bipolar cells. J. Neurosci. *19*, 2938–2944.

Pang, J.J., Gao, F., and Wu, S.M. (2004). Light-evoked current responses in rod bipolar cells, cone depolarizing bipolar cells, and AII amacrine cells in dark-adapted mouse retina. J. Physiol. *558*, 897–912.

Pardue, M.T., McCall, M.A., LaVail, M.M., Gregg, R.G., and Peachey, N.S. (1998). A naturally occurring mouse model of X-linked congenital stationary night blindness. Invest. Ophthalmol. Vis. Sci. *39*, 2443–2449.

Peachey, N.S., and Ball, S.L. (2003). Electrophysiological analysis of visual function in mutant mice. Doc. Ophthalmol. *107*, 13–36.

Pennesi, M.E., Cho, J.H., Yang, Z., Wu, S.H., Zhang, J., Wu, S.M., and Tsai, M.J. (2003a). BETA2/NeuroD1 null mice: a new model for transcription factor-dependent photoreceptor degeneration. J. Neurosci. *23*, 453–461.

Pennesi, M.E., Howes, K.A., Baehr, W., and Wu, S.M. (2003b). Guanylate cyclase-activating protein (GCAP) 1 rescues cone recovery kinetics in GCAP1/GCAP2 knockout mice. Proc. Natl. Acad. Sci. USA *100*, 6783–6788.

Pugh, E.N.J., Falsini, B., and Lyubarsky, A. (1998). The origin of the major rod- and cone-driven components of the rodent electroretinogram, and the effect of age and light rearing history on the magnitudes of these components. In Photostasis and Related Topics, T.P. Williams and A.B. Thistle, eds. (New York: Plenum), pp. 93–128.

Pusch, C.M., Zeitz, C., Brandau, O., Pesch, K., Achatz, H., Feil, S., Scharfe, C., Maurer, J., Jacobi, F.K., Pinckers, A., et al. (2000). The complete form of X-linked congenital stationary night blindness is caused by mutations in a gene encoding a leucine-rich repeat protein. Nat. Genet. *26*, 324–327.

Putcha, G.V., Deshmukh, M., and Johnson, E.M., Jr. (2000). Inhibition of apoptotic signaling cascades causes loss of trophic factor dependence during neuronal maturation. J. Cell Biol. *149*, 1011–1018.

Rice, D.S., and Curran, T. (2000). Disabled-1 is expressed in type AII amacrine cells in the mouse retina. J. Comp. Neurol. *424*, 327–338.

Rice, D.S., Nusinowitz, S., Azimi, A.M., Martinez, A., Soriano, E., and Curran, T. (2001). The reelin pathway modulates the structure and function of retinal synaptic circuitry. Neuron *31*, 929–941.

Sherry, D.M., Wang, M.M., Bates, J., and Frishman, L.J. (2003). Expression of vesicular glutamate transporter 1 in the mouse retina reveals temporal ordering in development of rod vs. cone and ON vs. OFF circuits. J. Comp. Neurol. *465*, 480–498.

Sterling, P. (1998). Retina. In The Synaptic Organization of the Brain, G.M. Shepherd, ed. (New York: Oxford University Press), pp. 205–253.Strom, T.M., Nyakatura, G., Apfelstedt-Sylla, E., Hellebrand, H., Lorenz, B., Weber, B.H., Wutz, K., Gutwillinger, N., Ruther, K., Drescher, B., et al. (1998). An L-type calcium-channel gene mutated in incomplete X-linked congenital stationary night blindness. Nat. Genet. *19*, 260–263.

Strettoi, E., and Pignatelli, V. (2000). Modifications of retinal neurons in a mouse model of retinitis pigmentosa. Proc. Natl. Acad. Sci. USA *97*, 11020–11025.

Strettoi, E., Dacheux, R.F., and Raviola, E. (1990). Synaptic connections of rod bipolar cells in the inner plexiform layer of the rabbit retina. J. Comp. Neurol. *295*, 449–466.

Strettoi, E., Raviola, E., and Dacheux, R.F. (1992). Synaptic connections of the narrow-field, bistratified rod amacrine cell (AII) in the rabbit retina. J. Comp. Neurol. *325*, 152–168.

Tagawa, Y., Sawai, H., Ueda, Y., Tauchi, M., and Nakanishi, S. (1999). Immunohistological studies of metabotropic glutamate receptor subtype 6-deficient mice show no abnormality of retinal cell organization and ganglion cell maturation. J. Neurosci. *19*, 2568–2579.

Vardi, N. (1998). Alpha subunit of Go localizes in the dendritic tips of ON bipolar cells. J. Comp. Neurol. *395*, 43–52.

Vardi, N., Matesic, D.F., Manning, D.R., Liebman, P.A., and Sterling, P. (1993). Identification of a G-protein in depolarizing rod bipolar cells. Vis. Neurosci. *10*, 473–478.

Wang, M.M., Janz, R., Belizaire, R., Frishman, L.J., and Sherry, D.M. (2003). Differential distribution and developmental expression of synaptic vesicle protein 2 isoforms in the mouse retina. J. Comp. Neurol. *460*, 106–122.

Young, R.W. (1984). Cell death during differentiation of the retina in the mouse. J. Comp. Neurol. *229*, 362–373.